Carrier Phase Airborne and Ground Monitors for Ionospheric Front Detection for Category III LAAS

L. Gratton and B. Pervan, *Illinois Institute of Technology*

ABSTRACT

The Federal Aviation Administration is currently developing the Local Area Augmentation System (LAAS) to transition from the current instrument landing system to satellite based navigation. Due to the single frequency nature of the current LAAS architecture, spatial ionospheric decorrelation contributes significantly to the differential ranging error during an approach. During days of normal ionospheric activity, the LAAS Ground Facility (LGF) broadcasts a conservative standard deviation of the spatial ionospheric gradient (σ_{vig}) to LAAS users. Under these normal circumstances, navigation integrity is ensured by incorporating σ_{vig} into the computation of position domain protection levels. However, anomalies exhibiting abrupt changes in the ionospheric gradient have been observed during ionospheric storms. Therefore, monitoring algorithms are necessary for LAAS to detect these hazardous ionospheric anomalies.

A three parameter (front width, gradient, and front speed) ionospheric threat model has been proposed and significant research has been devoted to the development and analysis of LGF and airborne code-carrier divergence monitors in the past. However, there are limitations on the effectiveness of these monitors, as they depend on the rate of change of the delay with time. The most hazardous threat in this regard is a static ionospheric wave front. In previous work a differential carrier phase Receiver Autonomous Integrity Monitoring (RAIM) was introduced evaluating its effectiveness for Category I approaches.

This work extends the analysis to Category III approaches, for the whole spectrum of fronts within the threat model, determining what combinations of widths and gradients are detectable, and what is the associated availability cost to ensure integrity.

Recent adjustments to the Threat model were taken into account. New algorithms to reduce computation time were also introduced, as the more stringent requirements for Category III made the algorithm running time prohibitive.

The availability loss incurred by the implementation of the carrier phase RAIM monitor is presented for different locations. It is shown that this loss is negligible for many width-gradient combinations. It is also shown it is tolerable for all width-gradients combinations if the monitor only operates during a storm alarm. Basic ideas on how this alarm could be triggered are mentioned in the paper

INTRODUCTION

The Federal Aviation Administration is currently developing its Differential GPS (DGPS) type implementation, the Local Area Augmentation System (LAAS) to transition from the current instrument landing system to satellite based navigation. Due to the single frequency nature of the current LAAS architecture, spatial ionospheric decorrelation between the LAAS Ground Facilities (LGF) antenna and the user contributes significantly to differential ranging errors. During days of normal ionospheric activity, the LGF broadcasts a conservative standard deviation of the spatial ionospheric gradient (σ_{vig}) to LAAS users. Under these normal circumstances, navigation integrity is ensured by incorporating σ_{vig} into the computation of position domain protection levels. However, anomalies exhibiting abrupt changes in the ionospheric gradient have been observed during ionospheric storms in October and November 2003 among others. During these occurrences, the ionospheric effect not eliminated by the broadcast range correction can potentially have a magnitude of tens of meters instead of the nominal centimeter level differences. Therefore, effective monitoring algorithms are necessary for LAAS to detect these hazardous ionospheric anomalies. It is desirable that these monitors don't affect the system's availability and continuity levels significantly.

Ionospheric fronts are very difficult to model, as the dynamics of their formation and change with time are not fully understood, and the quantity of data affected by

ionospheric fronts to analyze is limited. Stanford University developed a model that describes the front by its effect (delay) on the signal, and thus allows the front to be defined with only a few parameters, simplifying the analysis [1]. These parameters describe the shape of the front's edge (where the delay changes abruptly) and are:

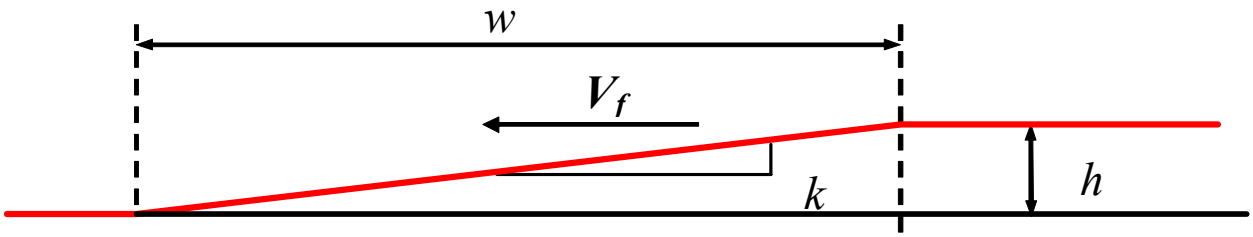

High Elevation /Moving Front (EL>12°)	Low Elevation /Moving (EL<12°)	Stationary (all elevations)
***w*: 25 – 200 km**	***w*: 25 – 200 km**	***w*: 25 – 200 km**
***k*: 30 – 400 mm/km**	***k*: 30 – 150 mm/km**	***k*: 30 – 125 mm/km**
V_f: 100 – 750 m/s	**V_f: 100-750**	**V_f: 0-100 m/s**
***Max Delay* (*h*) ≤ 50 m**	***Max Delay* ≤ 50 m**	***Max Delay* ≤ 30 m**

Figure 1: Ionospheric front edge model and threat space

the width (*w*), the vertical gradient (*k*), the height (*h*, derived from *w* and *k*), and the front's velocity. By considering the available data from various ionospheric storms, reasonable boundaries were defined for these parameters, obtaining a threat space. This threat space was recently modified, incorporating new data and better ways of analyzing it. A sketch of the model and the parameter values for the threat space are shown in figure 1. All values refer to slant delay.

Detection of these types of threats has been studied using ground and airborne variations of carrier-code divergence monitors. These monitors can mitigate the integrity risk for certain parts of the threat space, but as they depend on the rate of change of the delays, they do not work for slow varying fronts, or stationary fronts. The use of a ground monitor, using baselines between the existing antennas at the LGF to detect the ionospheric front gradient has also been studied. This type of monitor does not ensure detection either, as initial studies have shown that the noise in the measurements has to be smaller than what current technology provides, or the necessary baseline lengths would put antennas outside the LGF. Even if this was solved, the front could be between the LGF and the user, but not on top of the LGF, making detection impossible for the monitor

The monitor discussed in this paper is airborne, and it is a particular implementation of the Residual Autonomous Integrity Monitor (RAIM) that uses the very precise carrier phase measurements. This work intends to complete the results presented in [2], extending them to Category III approaches, explaining the particular challenges to meet its stringent requirements, and providing a detailed description of what combinations of widths and gradients for a static ionospheric front are detectable, and what is the associated availability cost to ensure integrity.

Having the results in terms of combinations of gradients and widths is very advantageous, as it gives insight on what specific front edge shapes are hazardous, and allows evaluating the performance of this monitor when combined with a ground baseline monitor. It also gives an idea of how the availability would change with adjustments to the threat model.

The purpose of the monitors is not to detect the ionospheric storm itself, but to detect if the storm is affecting a particular runway of an LGF site. This means that the availability losses from the monitors presented in this paper might apply only during a storm if there is a reliable ionospheric storm alarm system implemented. It is also worth noting that the hazardous situation for LAAS is not for the LGF and the user being in a high signal delay zone of a front, but when the delay at the LGF and the user's position is significantly different. This is why a failure on only one satellite at a time is considered, as the likelihood of two satellites simultaneously being on the edge of the front (as seen from the LGF and user) is considered negligible.

DIFFERENTIAL CARRIER PHASE RAIM MONITOR

The monitor works in two phases. Before initiating the approach, the user performs a geometry screening based on the probability of missed detection given a storm

(P_{MD}). If the geometry passes this test, at the LGF Broadcast Radius distance (x_{BR}) the user will compute a single difference user (A) - LGF (G) carrier phase measurement for each satellite i:

$$\phi_i^{SD0} = \phi_i^{A0} - \phi_i^{G0} \quad (1)$$

as it moves closer to the LGF, the user generates a double difference measurement in time.

$$\phi_i = \phi_i^{SD} - \phi_i^{SD0} \quad (2)$$

using a second differential carrier phase measurement. The Decision Height distance (x_{DH}) is the last point to detect a failure. This implementation uses the precise carrier phase to take differential measurements, taking advantage of the baseline formed by the airplane as it executes its approach. The values used in this analysis for x_{BR} and x_{DH} are 45 km and 5 km respectively. It must be stated that for the user to be able to compute these measurements, the LGF would need to broadcast carrier phase corrections (LAAS message Type 6).

Using the computed Line Of Sight unit vectors (LOS), the user will obtain a residual vector as:

$$\begin{bmatrix} r_1 \\ r_2 \\ \vdots \\ r_n \end{bmatrix} = \begin{bmatrix} \phi_1 \\ \phi_2 \\ \vdots \\ \phi_n \end{bmatrix} - \begin{bmatrix} -LOS_1 & 1 \\ -LOS_2 & 1 \\ \vdots & \vdots \\ -LOS_n & 1 \end{bmatrix} \begin{bmatrix} \Delta\hat{x} \\ \upsilon \end{bmatrix} = \phi - H\hat{u} \quad (3)$$

where the differential position vector $\Delta\hat{x}$ (in this case the vector with origin in the airplane's position at x_{BR} and ending in the x_{DH} position), and the clock bias υ are obtained from:

$$\hat{u} = (H^T V^{-1} H)^{-1} H^T V^{-1} \phi \quad (4)$$

with V being a time (t) changing diagonal weighting matrix whose elements are computed as:

$$\left(\sigma_i^t\right)^2 = 2\sigma_{SD}^2 + \left(\sigma_{vig} \times \Delta z_i^t \times Ob_i^t\right)^2 \quad (5)$$

σ_{SD}, is the single difference carrier phase measurement standard deviation (a nominal value of 1 cm is used in this work);

σ_{vig}, is the fault free vertical ionospheric gradient (4 mm/km).

Δz, is the distance between the pierce-points of the two airplane-SV measurement rays (one at BR and one at DH distance), and

Ob, is the obliquity factor.

The time superscript is dropped from now on.

The test statistic for this monitor will be similar to the one in a Residual Autonomous Integrity Monitor (RAIM) implementation: the norm of the residual vector, now weighted using (5):

$$r = \left\| \begin{bmatrix} \frac{r_1}{\sigma_1} & \frac{r_2}{\sigma_2} & \cdots & \frac{r_n}{\sigma_n} \end{bmatrix} \right\| \quad (6)$$

The Monitor compares r with a threshold T obtained from the continuity constraint [2]. If $r > T$, the approach is aborted. Integrity is thus provided by the geometry screening, and continuity is provided by the way T was computed. The efficiency of the monitor is then evaluated by the availability loss incurred in the geometry screening.

RAIM AND THE SLOPE MODIFIER α

In case of a failure caused by an ionospheric storm, its impact on the test statistic r will be [2]:

$$r^I = \left(I_d - HH^*\right)_{:,i} \left(d_{i(DH)} - d_{i(BR)}\right) \quad (7)$$

where:

I_d, is the identity matrix

H^*, is the pseudoinverse of H, weighted with matrix V (4) and;

d_i, is the bias introduced in the carrier phase single difference measurement for satellite i by the ionospheric front.

The vertical position error caused by the failure will be:

$$\delta x_v^I = H_{3,i}^+ f_{i(DH)}^I \quad (8)$$

where:

H^+, is the pseudoinverse of H weighted according to the differential carrier smoothed code specifications for LAAS [3], and

f_i^I, is the error accumulated in the differential Hatch filter measurement to satellite i.

Both effects (on the vertical position error and on the residual) have been considered at decision height distance, as it has the most stringent Vertical Alert Limit (VAL).

The P_{MD} given a failure F^I, (which will be a function of w, k, and the obliquity factor Ob) is:

$$P_{MD} = P(\delta x_v > VAL) \times P(r < T) \left| F^I(w,k,Ob) \right. \quad (9)$$

In a traditional RAIM approach, (for a generic failure F) the Failure Mode Slope is defined as:

$$FMS = \frac{\left|\delta x_v^F\right|}{\left\|r^F\right\|} = \frac{\left|H_{3,i}^+\right|}{\left\|(I - HH^+)_{:,i}\right\|} \frac{F}{F} \quad (10)$$

It is used to determine availability. For each geometry, a plot of vertical error δx_v with respect to the norm of the residual can be generated (figure 2), where the slope of a line is defined by the FMS, and the nominal distribution or fault free "noise" is schematically represented by the ellipses. The location along this line where the P_{MD} is the biggest (darker ellipse in the figure) can be obtained. If that P_{MD} is bigger than the integrity threshold that geometry is discarded.

When Carrier phase RAIM is use to detect ionospheric fronts, additional complications need to be considered. A closer look at the vertical position error and the residual r (7) and (8) when there is an ionospheric storm shows that the magnitude from F^I affecting r:

$$\Delta d_i^I = d_{i(DH)} - d_{i(BR)} = (w - x_{DH}) \times k \times Ob \quad (11)$$

and the magnitude affecting δx_v:

$$f_{i(DH)}^I = k \times Ob \times \left[x_{DH} + 2v\tau \left(1 - e^{-\frac{w - x_{DH}}{vx}} \right) \right] \quad (12)$$

are no longer equal (see [2] for details). Now the failure magnitudes to consider are represented in figure 2 by the whole plane instead of a line. Once the limits in k, w and maximum delay of the threat space are applied, the points to evaluate for a given satellite and geometry become an area in the plane (figure 3). It is obvious that finding the point with the worst P_{MD} is now more difficult. Moreover, it is not the maximum that we want to find, but the limits of the colored area in figure 3 for which the P_{MD} exceeds the integrity constraint ($P_{MDreq}=10^{-6}$ in the Category III ionospheric storm evaluation).

The aim is then to fill a matrix for each geometry (table 1) in which each element (corresponding to a different w, k combination) will be filled with an unavailable result (U) if for any satellite in that geometry the $P_{MD} > 10^{-6}$, and the geometry will be available (A) for that particular threat if for all SV's $P_{MD} < 10^{-6}$. Following this process for each time of interest, adding all matrices (U=0 and A=1), and dividing by the number of geometries, the

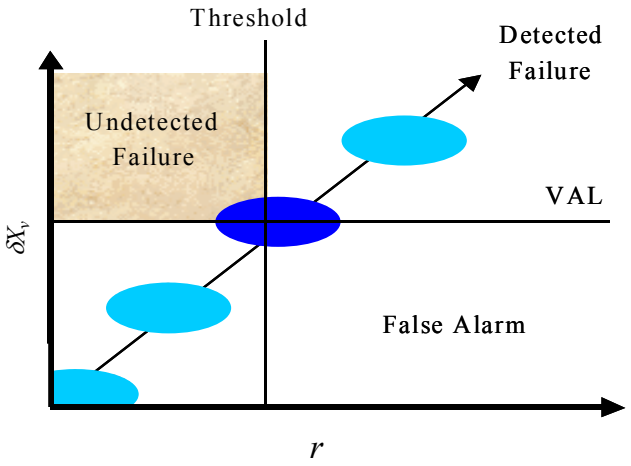

Figure 2: FMS and PMD

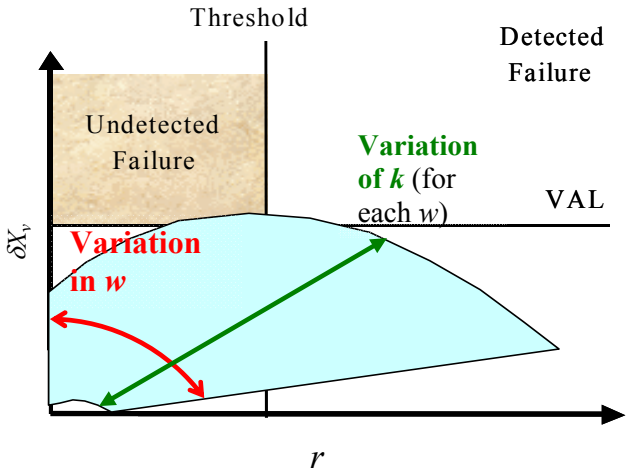

Figure 3: Carrier phase RAIM failure space

k / w	30 mm/km	40 mm/km	50 mm/km	…	250 mm/km
0 km	A	A	A	…	A
10 km	A	A	U	…	U
…	…	…	…	…	…
200 km	A	U	U	…	A

Table 1: Availability matrix for each geometry (example)

k / w	30 mm/km	40 mm/km	50 mm/km	…	200 mm/km
0km	99.99%	99.97%	99.7%	…	99.99%
10km	99.98%	99.97%	82%	…	99.98%
…	…	…	…	…	…
250km	99,80%	99.75%	99.74%	…	99.99%

Table 2: Availability matrix for all geometries (example)

final availability result is obtained in the form of table 2. The amount of computation needed for this task is enormous. This computation burden requires some way of reducing the number of points to evaluate. In order to do this, the advantageous representation of a line from the traditional RAIM has to be recovered. This can be achieved by fixing w. By first defining a slope modifier α_w as:

$$\alpha \equiv \left| \frac{f^I_{i(DH)}}{\Delta d^I_i} \right| = \frac{x_{DH} + 2v\tau\left(1 - e^{-\frac{w - x_{DH}}{vx}}\right)}{w - x_{DH}} \quad (13)$$

(where the *Ob* and k are cancelled); the FMS for each w can be redefined as:

$$FMS_w \equiv \frac{\left|\delta x^I_v\right|}{\left\|r^I\right\|} = \frac{\left|H^+_{3,i}\right|}{\left\|(I - HH^*)_{:,i}\right\|} \frac{f^I_i}{\Delta d^I_i} = \alpha_w \frac{\left|H^+_{3,i}\right|}{\left\|(I - HH^*)_{:,i}\right\|} \frac{\Delta d^I_i}{\Delta d^I_i} \quad (14)$$

As the failures in the numerator and the denominator are equal again, changing its magnitude will slide the point up and down a line with slope FMS for each particular width. The line visualization is recovered with all its advantages. The most obvious one is that only the satellite with the worst FMS needs to be evaluated.

THREAT SPACE COMPUTATION REDUCTION

In previous work [2] it was described how to reduce the number of points to be computed in table 1, either because the result is obvious without need of computing the P_{MD} for those points, or because it can be deduced from a previously computed result. As the details of the implementation are not necessary to understand the results, they are only described schematically, with the details being in [2], and in Appendix A.

It was shown in [2] that (9) only needs to be evaluated for 5 km $<w<$44.9 km, and the availability for the rest of the threat space's widths can be derived from those results, by using conservative approximations.

It was also shown how for each line evaluated (corresponding to one value of w) the minimum k to be considered (k_{min}) can be obtained by assuming no detection, and the maximum k to be considered (k_{max}) is obtained by assuming the vertical error is always larger than the VAL. That was a major step in reducing the computation time, because for low slope lines, $k_{max}<k_{min}$ making it obvious for the algorithm that no evaluation is needed as no value of k makes the geometry unavailable for that w.

The last step to reduce the computation time, and the most significant one, was finding the largest interval (Δk) between values of k to be evaluated in each line. As the way of finding this interval is different than the one used for generating Category I results, it is explained in detail in Appendix A. The implementation of these concepts allowed reducing the computation time from months to a few days per site.

CONSTELLATION

The constellation used is the same as the one used to generate the Cat I results in our previous work. The period considered was the whole year 2004. For that period, the Coast Guard NANUS were consulted, establishing all cases in which a satellite was added or taken out of the GPS constellation [2]. For each lapse of time without changes in the number of SV's, a set of broadcast ephemerides close to the middle point of that period was used to generate the satellite positions for that lapse of time. This has the advantage of giving a real sense of the impact of the monitor implementation with the actual satellites in space and their outages. It also has the added value, that for segments of time bigger than a sidereal day, only the availability matrices (table 1) for the first 24 hours need to be computed as the results will be repeated in a daily basis. The sample interval was 4 minutes.

RESULTS

The unavailability in percentage for 3 of the sites evaluated is shown in figure4. Results are coincident with what would be expected from the analysis. It can be observed that there is an intermediate range of combinations of w and k for which there is some availability loss. If the magnitude of the failure is smaller, it won't cause a vertical position error large enough to be a threat, and if it is too large it will always be detected by the RAIM residual test. Results also show that an antenna baseline monitor on the ground would not add much to the availability, unless it could detect fronts with a k of less than 40 mm/km. [Note: At the moment of the generation of these results, the ground monitor was generally assumed to detect fronts with k>150mm/km]

The total unavailability is defined as the availability loss resulting from discarding any geometry for which one or

more combinations of w and k has a $P_{MD} > P_{MDreq.}$ Table 3 shows the results for the sites evaluated. For all of them the availability loss is less than 0.55%.

It is important to note that this impact on availability would only occur during a storm if a reliable storm alarm system is implemented. The alarm for the storm could come from WAAS. Another interesting option is using NASA's satellites located between the earth and the sun.

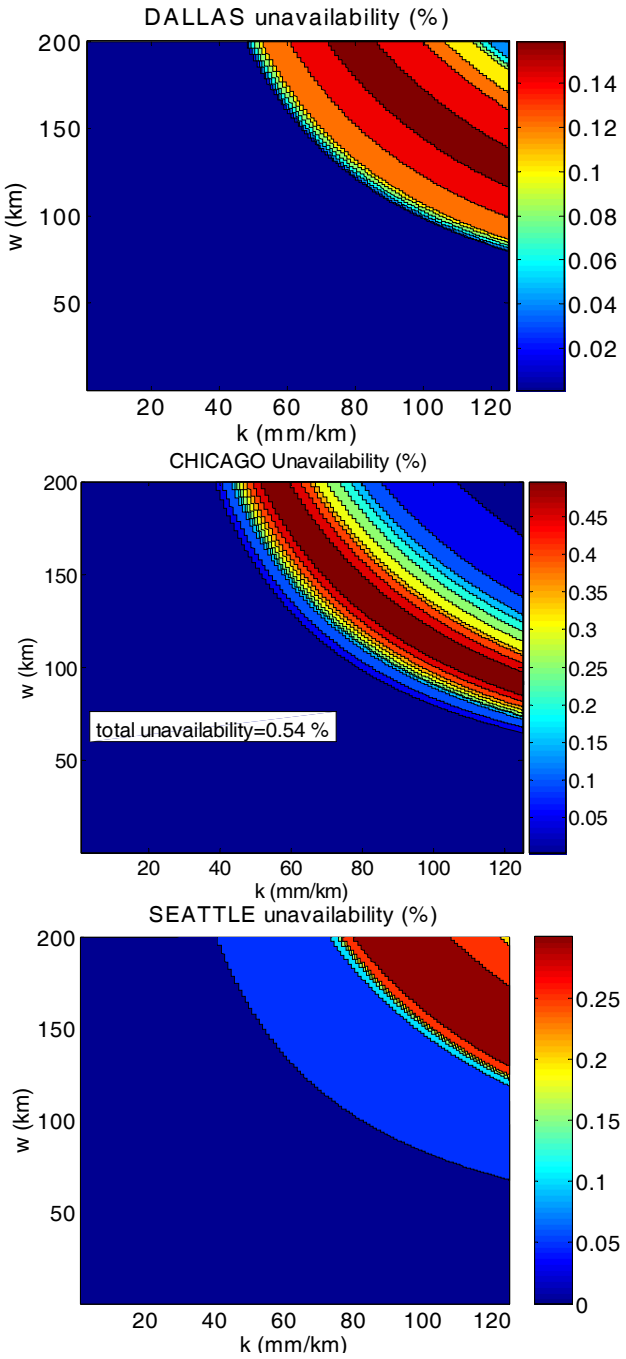

Figure 4: Geometry screening unavailability

	Total Unavailability
Chicago	0.54 %
Dallas	0.17 %
New York	0.52 %
Miami.	0.1 %
London	0.04 %
Seattle	0.46 %
Panama	0.36 %

Table 3: Final RAIM availability results

ACE, in a halo type orbit around the L1 libration point, can provide accurate information determining if a Coronal Mass Ejection (CME) from the sun will affect the earth's ionosphere with at least an hour warning, while SOHO can provide a less accurate early warning a few days before the CME impacts the atmosphere. Once STEREO is in orbit, the number of false early warnings will be significantly reduced [4].

CONCLUSSIONS

The static front is the most hazardous type of ionospheric anomaly, as existing monitors cannot detect it. A RAIM type monitor algorithm was described. It takes advantage of the baseline formed by the aircraft's movement during the final approach, and the precision of the carrier phase measurements utilized in its implementation. As a tradeoff, it requires the broadcast of message type 6 (carrier phase corrections), and the evaluation of the P_{MD} for geometry screening is more sophisticated. The computational burden to estimate the availability loss was reduced significantly by using the properties of the distributions for the RAIM residual and the aircraft's position error, making it a realizable task time-wise. A new way of computing the availability loss was introduced using the actual GPS constellation in the sky during a whole year. If the RAIM monitor operates in conjunction with an LGF baseline monitor, the availability would not be significantly increased unless the ground monitor is able to detect gradients smaller than 40 to 70 mm/km depending on the site. For a range of representative sites, results show that using the new slant delay threat space, the total availability loss from the RAIM monitor's geometry screening varies from 0.04 to 0.54 %. The availability loss is tolerable for all front width-gradient combinations, if the monitor only operates during a storm alarm

APPENDIX A: Search interval (Δk) computation

For each line with a FMS corresponding to a certain geometry and width, the P_{MD} has to be evaluated for a

segment from k_{min} to k_{max}. Our purpose is to avoid having a Δk that is too large, as to risk "missing" a value of k for which $P_{MD} > P_{MDreq}$, making available points that really should be discarded. On the other hand, as Δk is made smaller, more points need to be computed, so it is desirable to make is as large as possible.

The P_{MD} comes from multiplying 2 probabilities (9). As the CDF of $P(\delta x_v > VAL)$ is a monotonically increasing function with k, and the CDF of $P(r < T)$ is a monotonically decreasing function with k, there can be a maximum of 2 values of k that give the same P_{MD}. This allows us to state that if we choose a $P_{MDsearch} > P_{MDreq}$, no point with $P_{MD} > P_{MDreq}$ exists between $k_{min}$and k_{max} if no point with $P_{MD} > P_{MDsearch}$ is found in our evaluation, and

$$\Delta k < k_{req} - k_{search} \qquad \text{(A1)}$$

where k_{req} and k_{search} are the values of k that give a P_{MDreq} (in this work 10^{-6})and $P_{MDsearch}$ (in this work 10^{-5}) respectively.

Again using the monotonic properties of the individual probabilities that produce P_{MD}, it can be stated that the rate of change in the P_{MD} curve can never be bigger than any of the two individual rates at that point (as the individual rates are always in opposite directions).

The idea is to identify the point with the highest rate of change in each of the individual curves, select the higher of these two, and in that point compute the Δk necessary to produce a change in $P(\delta x_v > VAL)$ or $P(r < T)$ (depending what curve we are looking at) that is equal to $\Delta P = P_{MDreq} - P_{MDsearch.}$ Given the property stated in the previous paragraph, the Δk found this way complies with the condition in (A1).

The biggest rate of change of a Gaussian CDF is at the 0.5 point. In this work we can assume that for a non central Chi^2 distribution the non centrality parameter in big enough as to make the maximum change also close to the 0.5 point. The curvature also changes at that point. The rate of the rate of change goes from positive to negative for the Gaussian, and from negative to positive for the Chi^2 distribution [Note: $P(r < T)$ is actually given by 1-CDF of a Chi^2 distribution. It is the CDF of $P(r < T)$ that we are referring to when we talk about a "Chi^2" or "non central Chi^2" distribution]. The only interval of interest is between k_{min} and $k_{max.}$.

The procedure to find Δk is as follows:

The $P(\delta x_v > VAL)$ and the $P(r < T)$ are evaluated both at k_{min} and $k_{max.}$ Depending on the result, the following cases need to be analyzed. [For each case, Δk is evaluated at the point with the steepest slope in the individual curves. That guarantees that when we apply Δk on the P_{MD} search, we are being conservative, in other words that in complies with (A1)]:

If for both curves one P is lower than 0.5, and the other one is higher, then Δk must be evaluated at the point in the curve were P is 0.5 (which is not difficult to find for the individual curves). This is the case shown in figure A1 (Note: Figure is out of scale to allow visualization. All values of "k" should be read in the x axis), where:

k_+^{Chi} is the k that produces a

$$P(r < T) = 0.5 + \frac{P_{MDsearch} - P_{MDreq}}{2} \quad \text{and}$$

k_-^{Chi} is the k that produces a

$$P(r < T) = 0.5 - \frac{P_{MDsearch} - P_{MDreq}}{2}$$

k_+^{Gauss} is the k that produces a

$$P(\delta x_v > VAL) = 0.5 + \frac{P_{MDsearch} - P_{MDreq}}{2} \quad \text{and}$$

k_-^{Gauss} is the k that produces a

$$P(\delta x_v > VAL) = 0.5 - \frac{P_{MDsearch} - P_{MDreq}}{2}$$

If all 4 points give a P > 0.5, then Δk is evaluated at k_{min} for the Gaussian, and at k_{ma} for the Chi^2 distribution:

k_+^{Chi} is the k that produces a

$$P(r < T) = P_{k_{\max}} + \frac{P_{MDsearch} - P_{MDreq}}{2} \quad \text{and}$$

k_-^{Chi} is the k that produces a

$$P(r < T) = P_{k_{\max}} - \frac{P_{MDsearch} - P_{MDreq}}{2}$$

k_+^{Gauss} is the k that produces a

$$P(\delta x_v > VAL) = P_{k_{\min}} + \frac{P_{MDsearch} - P_{MDreq}}{2} \quad \text{and}$$

k_-^{Gauss} is the k that produces a

$$P(\delta x_v > VAL) = P_{k_{\min}} - \frac{P_{MDsearch} - P_{MDreq}}{2}$$

If all 4 points give a P < 0.5, then Δk is evaluated at k_{min} for the Chi^2 distribution, and at k_{max} for the Gaussian. For this case, the

k_+^{Chi} is the k that produces a

$$P(r < T) = P_{k_{\min}} + \frac{P_{MDsearch} - P_{MDreq}}{2}$$ and

k_{-}^{Chi} is the k that produces a

$$P(r < T) = P_{k_{\min}} - \frac{P_{MDsearch} - P_{MDreq}}{2}$$

k_{+}^{Gauss} is the k that produces a

$$P(\delta x_v > VAL) = P_{k_{\max}} + \frac{P_{MDsearch} - P_{MDreq}}{2}$$ and

k_{-}^{Gauss} is the k that produces a

$$P(\delta x_v > VAL) = P_{k_{\max}} - \frac{P_{MDsearch} - P_{MDreq}}{2}$$

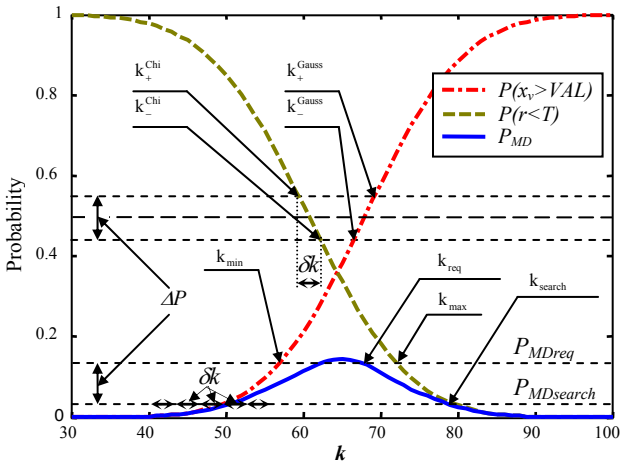

Figure A1: Search interval computation

If the results are a mix of these cases, the rules in the paragraphs above are applied to each individual curve accordingly.

This procedure allows discarding a k_{req} exists at all for a given geometry and w in a reasonable time. If it is found it exists, finding the limits where $P_{MD} > P_{MDreq}$ is not time consuming.

ACKNOWLEDGMENTS

The authors wish to acknowledge Sam Pullen and Ming Luo for their useful comments on the threat model and the specifications to be used, Mathieu Joerger for his comments and help with the plots, and the Federal Aviation Administration for sponsoring this research.

REFERENCES

[1] Luo, Ming, L., Pullen, S., Walter, T., and Enge, P., "Ionosphere Spatial Gradient Threat for LAAS: Mitigation and Tolerable Threat Space", Institute of Navigation's National Technical Meeting, San Diego CA 2004

[2] L., Gratton, B., Pervan; "Airborne and Ground Monitors for Ionospheric Front Detection in LAAS Using Carrier Phase", Institute of Navigation's National GNSS Meeting, Long Beach, CA 2005

[3] "Minimum Aviation System Performance Standards for the Local Area Augmentation System" RTCA Paper No.037-98/SC159-778, February 1998

[4] "The Sun and The Heliosphere in Three Dimensions", Report of the NASA Science Definition Team for the STEREO Mission, 1997